JGR 103(D24):32215-32238, 1998

http://www.cstars.ucdavis.edu/papers/html/kaufmanetal1998a/index.html

Potential Global Fire Monitoring from EOS-MODIS

The MODIS Fire Science Team:
Yoram J. Kaufman[1], Chris Justice[2], Luke Flynn[3], Jackie Kendall[4] , Elaine Prins[4,] Louis Giglio[5], Darold E. Ward[6], P. Menzel[7] and A. Setzer[8]

[1]NASA/Goddard SFC, Laboratory for Atmospheres (Code 913), Greenbelt MD 20771
[2]Dept. of Environmental Sciences, University of Virginia, Charlottesville VA 22903
[3]Hawaii Inst. of Geoph. and Planet., U. of Hawaii, 2525 Correa Rd, Honolulu, HA 96822
[4]Cooperative Institute for Meteorological Satellite Studies, University of Wisconsin Madison, 1225 West Dayton St., Madison, WI 53706
[5]Science Systems and Applications Inc., 5900 Princess Garden Parkway, Lanham, MD 20706
[6]Intermountain Research Station, U.S. Forest Service, USDA, Missoula, MT 59807
[7]NOAA/NESDIS, 1225 West Dayton St., Madison, WI 53706
[8]INPE C. Postal 515, 12201 S.J. Campos - SP, Brazil

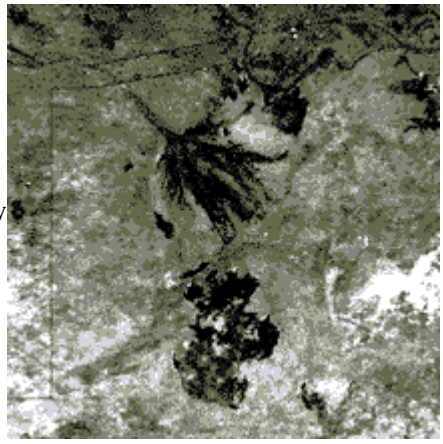

Abstract

The National Aeronautic and Space Administration (NASA) plans to launch the Moderate Resolution Imaging Spectroradiometer (MODIS) on the polar-orbiting Earth Observation System (EOS) providing morning and evening global observations in 1998 and afternoon and night observations in 2000. These four MODIS daily fire observations will advance global fire monitoring with special 1 km resolution fire channels at 4 μm and 11 μm, with high saturation of about 450 K and 400 K, respectively. MODIS data will also be used to monitor burn scars, vegetation type and condition, smoke aerosols, water vapor and clouds for overall monitoring of the fire process and its effects on ecosystems, the atmosphere and the climate.

The MODIS fire science team is preparing algorithms that use the thermal signature to separate the fire signal from the background signal. A data base of active fire products will be generated and archived at a 1 km resolution and summarized on a grid of 10 km and 0.5° - daily, 8 days and monthly. It includes the fire occurrence and location, the rate of emission of thermal energy from the fire and a rough estimate of the smoldering/flaming ratio. This information will be used in monitoring the spatial and temporal distribution of fires in different ecosystems, detecting changes in fire distribution and identifying new fire frontiers, wild fires, and changes in the frequency of the fires or their relative strength. We plan to combine the MODIS fire measurements with a detailed diurnal cycle of the fires from geostationary satellites.

Sensitivity studies and analyses of aircraft and satellite data from the Yellowstone wild fire of 1988 and prescribed fires in the Smoke Cloud and Radiation (SCAR) aircraft field experiments are used to evaluate and validate the fire algorithms and to establish the

relationship between the fire thermal properties, the rate of biomass consumption and the emissions of aerosol and trace gases from fires.

1. Introduction

Biomass burning is a major source of trace gases and aerosol particles, with significant ramifications for atmospheric chemistry, cloud properties and radiation budget (Crutzen et al., 1979; Crutzen and Andreae, 1990; Kaufman et al., 1992). Biomass burning accounts for about a quarter of the global emissions of greenhouse gases, with comparable rate of production of smoke particles to that of sulfate particles from industrial and urban sources (Radke et al., 1991; Penner et al., 1992; IPCC, 1995). Smoke particles have been shown to be effective cloud condensation nuclei (Warner and Twomey, 1967; Hobbs and Radke, 1969), affect the cloud drop size and reflectivity (Kaufman and Nakajima, 1993; Kaufman and Fraser, 1997) and may have a similar radiative forcing to that of sulfates (Penner et al., 1992; Dickinson, 1993). Though Hobbs et al. (1997) showed that due to its low sensitivity to humidity and high absorption the effect may be significantly smaller. The combined effect of biomass burning aerosols and aerosols originating from industrial/urban activities is considered to be the largest identified uncertainty in assessing a possible anthropogenic climate change (Hansen and Lacis, 1990; IPCC, 1995).

Fire is also a significant and periodic factor in the ecology of savannas, boreal forests and tundra, and plays a major role in deforestation in tropical and sub-tropical regions. On a periodic basis, extensive fires also occur in many temperate biomes such as forests, grasslands, and chaparral. Fire is an integral part of land management in many parts of the World, particularly in the tropics. Following the pioneering work by Crutzen et al. (1979) on the importance of biomass burning in the tropics over two decades ago, a large effort has been exerted to address this atmospheric process (see review by Crutzen and Andreae, 1990). However, there are no accurate estimates of the global sources and emissions from biomass burning to date. The traditional approach, and that adopted as the Intergovernmental Panel on Climate Change (IPCC) methodology for national emission estimates, is based on the Food and Agricultural Organization (FAO) statistics on population and agricultural practices (Hao, 1994, Skole et al. 1994). Other assessments use operational remote sensing of fires (Setzer and Pereira, 1991) from the polar orbiting NOAA (National Oceanic and Atmospheric Administration) AVHRR sensor. Simultaneous remote sensing of smoke and fires were suggested by Kaufman et al. (1990a and b; 1994). New approaches are also emerging, that incorporate remote sensing of burn scars left by fires (Justice et al, 1996; Kendall et al., 1997; Roy et al., 1997).

In this paper, the heritage of remote sensing of fires from satellites, the limitations in the present satellite capability and the strategy in the design of the MODIS sensor and the MODIS fire detection algorithm will be reviewed.

2. The Heritage for Fire Remote Sensing

Regional remote sensing of fires can be achieved using the Visible Atmospheric Sounder (VAS) sensors on the Geostationary Orbiting Environmental Satellite (GOES) platforms

and the polar orbiting NOAA AVHRR sensors. The VAS can be used to locate active fires by utilizing the visible, 4 μm, and 11 μm data. Since 1980 the VAS instruments on GOES 4-7 have provided multispectral monitoring of the Western Hemisphere. The GOES, positioned at a height of 36,000 km at a fixed point above the Equator, has the advantage of sensing the Earth and fires diurnally. GOES VAS was scheduled to monitor fires at most every 3 hours with a spatial resolution at 4 μm and 11 μm of 7 and 14 km, respectively. GOES-8, launched in 1994, increased the temporal (every 15 minutes in North America, half-hourly elsewhere) and spatial resolution (4 km in the infrared bands), thus enabling improved detection of fire characteristics and aerosol loading and transport (Menzel and Prins, 1996; Prins and Menzel, 1996a). Prins and Menzel (1992; 1994) developed an automated algorithm to detect fires and determine the sub-pixel size of the active fire(s) and average fire temperature based on an adaptation of an algorithm proposed by Dozier (1981).

The GOES Automated Biomass Burning Algorithm (ABBA) is a dynamic multispectral thresholding algorithm which utilizes regional thresholds derived from the satellite data (visible, 4 μm, and 11μm) for fire pixel identification and incorporates ancillary data to correct for water vapor attenuation, surface emissivity, and solar reflectivity. Figure 1 shows examples of GOES-8 fire detection in the Northwest United States. GOES-8 observations of individual fires during the Smoke Cloud and Radiation (SCAR-C) field experiment based in California were verified using aircraft and field observations (Menzel and Prins, 1996). Several prescribed burns (Figure 1a) were initiated on 21 September 1994 in Washington in association with the SCAR-C experiment, including the Quinault fire (48 acres), the Simpson fire (95 acres), and the ITT fire (97 acres). The fires outlined in Figure 1b represent wildfires in Northern California which were evident in the GOES-8 imagery over several days during SCAR-C. Figure 2 provides an example of GOES-8 ABBA diurnal fire monitoring results for August 24 1995, one of the peak burning days during the Smoke Cloud and Radiation (SCAR-B) field experiment in Brazil. Throughout SCAR-B the number of fire pixels detected daily in South America with the GOES-8 ABBA at 1745 UTC ranged from 100 to over 3500. This was on average two to four times greater than that observed 3 hours earlier or later and 20 times greater than that observed at 1145 UTC (Prins and Menzel, 1996b).

Additional information on the global distribution of nighttime fires can be obtained from the visible low-light sensors of the Operational Linescan System (OLS) on the Defense Meteorological Satellite Program (DMSP) (Cahoon et al. 1992, Elvidge et al. 1996).

The current sequence of NOAA Polar Orbiting Environmental Satellites (NPOES) has been in continuous operation since October 1978. They include the AVHRR which is a scanning radiometer measuring reflected and emitted radiation in five channels, two of which are used for fire detection (3.75 μm and 11 μm). On-board calibration uses measurements of deep space and a black-body of known temperature. Unfortunately, these channels, developed for observation of clouds and ocean temperature, saturate at 325 K. A non-linearity in their response and even a folding of the values around the saturation temperature was discovered, limiting the success in the application of detection and inversion algorithms (Setzer and Verstrate, 1994). The viewing geometry gives rise to a 1.1 km ground resolution for pixels at nadir, similar to the planned MODIS infrared channels.

The wide scan angle (55°) leads to pixels at the edge of the scan being ten times over the size of pixels at nadir, and overlapping each other considerably. An example of NOAA AVHRR 1 km fires and burn scars observed for the Okavango Delta of Botswana is provided in Figure 3.

Dozier (1981) introduced a theoretical approach to study sub-pixel temperature fields using the 3.7 and 11 μm channels. He approximated the temperature field of each pixel by two areas of uniform temperature: the background area and a target area which occupies some fraction from 0 to 1 of the pixel. Using his model, Dozier was able to show that a sub-resolution high temperature target is detectable because it has a greater effect in the 3.7 μm channel than in the 11 μm channel. He also derived equations that could be solved for the temperature and the size of the hot target given the background temperature and the brightness temperatures at 3.7 and 11 μm. These equations were restricted to pixels that are unsaturated in both channels and the fire is strong enough to have a significantly larger impact on the 11 μm channel than the background variability. This limits the applicability of this approach. Dozier also suggested using a split-window technique to calculate a correction factor for the effect of atmospheric water vapor on the inversion.

The first applications of fire detection with AVHRR data were on fixed targets of known location. Matson and Dozier (1981) used NOAA-6 nighttime imagery to detect high temperature industrial sources in Detroit and waste gas flares in the Persian Gulf. Similarly, Muirhead and Cracknell (1984) detected gas flares associated with oil fields in the North Sea using daytime NOAA-6 data. Following these studies of fixed targets, the AVHRR was used to detect vegetation fires. Matson et al. (1984) used daytime NOAA-6 and 7 imagery over the U.S. and Brazil to detect fires based on enhanced temperatures in the 3.7 μm channel. They also reported on an operational fire monitoring project in the western U.S. that was based on manual inspection of the 3.7 μm and 11 μm images alternating on a screen. More importantly, these detections were largely verified by U.S. Forest Service stations, timber companies and local police. Muirhead and Cracknell (1984) also applied their fire detection technique to detect straw-burning in Great Britain using daytime NOAA-7 imagery.

Flannigan and Vonder Haar (1986) and Flannigan (1985) developed the first automated (i.e., non-interactive) set of fire detection criteria. They used both daytime and nighttime data from NOAA-7 to monitor a severe forest fire outbreak in north-central Alberta, Canada. They were able to compare and validate satellite detections with Alberta Forest Service daily reports of fire location and size, using late afternoon aerial reconnaissance. Using their detection criteria they were able to identify 80% of the 41% of fires that were visible to the satellite (unobstructed by clouds). The AVHRR-based fire size estimates were 70% larger for small fires and 50% smaller for large fires compared with the reconnaissance information. A number of case studies were also reported from diverse regions (Matson et al., 1987; Matson and Holben, 1987; Stephens and Matson, 1989; Langaas and Muirhead, 1989). These studies included an increasingly sophisticated discussion of limitations and problems associated with fire detection using the AVHRR. This included effects of fixed, non-fire sources (Stephens and Matson, 1989), detection of and fire obscuration due to smoke plumes (Matson et al., 1987; Matson and Holben, 1987), and effects of surface emissivity, pixel overlap at non-nadir scan angles and incorporation

of recently burnt warm areas into the two-element temperature field of the Dozier model (Langaas and Muirhead, 1989).

Lee and Tag (1990) presented an alternative approach to non-interactive fire detection examining nighttime imagery over the San Francisco area and the Persian Gulf. They subjectively chose a threshold fire temperature and used the Dozier model to develop a look-up table specifying which combinations of satellite measurements constituted a positive fire detection. Atmospheric corrections were included in the estimation of background temperatures using the method of McClain et al. (1985).

The saturation of the AVHRR 3.7 μm channel prohibits distinction between small and large fires and between smoldering and flaming fires. In order to use AVHRR fire detection in regional assessments of emissions from fires, Kaufman et al. (1990a, b) applied fire and smoke detection from NOAA-9 data. Fires were identified for pixels that met three detection criteria. The first criterion was that the 3.7 μm channel brightness temperature would be elevated above a set threshold indicating a fire is present. The second criterion specified that the difference between the 3.7 μm and 11 μm temperatures should be at least 10 K, to avoid hot exposed soils. The third criterion used the 11 μm temperature for elimination of false detections from cool clouds with small drop sizes that are highly reflective in the 3.7 μm band. In regions where the smoke was clearly identified to originate from specific groups of fires, the average emission of particulates per fire was calculated and used to convert the total seasonal number of fires into an emission estimate.

Justice et al. (1996) and Scholes et al. (1996) combined AVHRR fire information in a dynamic model to provide improved trace gas and particulate emissions estimates for Southern Africa. The approach combined satellite data on fire distribution and timing with fuel load calculated by a simplified ecosystem production model and ground based measurements of emission ratios (Ward et al. 1996, Shea et al. 1996). Daily fires detected by the AVHRR for the entire burning season were calibrated to provide burned area estimates using Landsat Multispectral Scanner (MSS) data. The algorithm used for fire detection is described by Kendall et al. (1997) and is the basis for the IGBP-DIS community consensus algorithm for the AVHRR. This trace gas modeling was part of a larger body of fire related research undertaken as part of the IGBP Southern African Fire Atmosphere Research Initiative (SAFARI) (Andreae et al., 1994; Thompson, 1996). The fire data generated from the AVHRR were used to better understand trace gas trajectories and atmospheric chemistry (Thompson et al., 1997).

Setzer and Pereira (1991) started the first regional operational fire monitoring program in Brazil. Since 1989 they have been monitoring fire occurrence for each fire season. Using NOAA-11 data in 1989, 96% of the detected fires were verified by ground crews and there were no reports of missing fires. Setzer and Pereira (1991) adopted a fixed 3.7 μm temperature threshold to flag potential fires but, in addition, required that smoke plumes are identified by manual inspection of imagery in the AVHRR 0.64 μm channel in order to have positive detection. Pereira et al. (1991) used AVHRR data from five consecutive days and Landsat/TM data from the sixth day to evaluate the accuracy of fire detection and burned area estimates. All AVHRR-detected fires had corresponding TM burn scars. They found that, on average, the fire size was 43% of the AVHRR pixel size. Pereira and Setzer

(1993) detected deforestation fires using a fixed 3.7 μm threshold applied to raw digital counts instead of derived brightness temperatures. A summary of the main advantages and limitations of the AVHRR technique can be found in Setzer (1994) and Setzer and Malingreau (1996).

Figure 4 shows a sequence of maps with the number of AVHRR fire pixels detected over Brazil each month of the unusually dry season of 1991, when extensive burning took place. The monthly total number of fire pixels for Brazil in 1991 are summarized in Table 1. The peak in fire activity occurs usually in the last two weeks of August and the first week of September and almost all fires are of anthropogenic origin. The last map shows the cumulative fire activity for the season with about 470 thousand fire pixels; a high concentration of fires is observed along the southern boundary of the Amazon Basin where conversion of natural forests and savannas to agriculture and pasture land is taking place. A northward progression of fire activity associated with the advance of the dry season is clearly shown in the monthly sequence of imagery.

Similar data also exists for other years, allowing a more extended analysis. Utilizing the same kind of time series data, the total number of fire pixels for the June-October period of 1992 to 1994 is summarized in Table 1. Large annual variations are evident. In 1995, the data are shown through August 17, where a change of satellites on August 18 from the early afternoon pass of NOAA-14 to the early night images of NOAA-12, corresponds to a strong reduction in the fire count. Most fires in Brazil are started in the afternoon to take advantage of dryer air in order to obtain higher combustion efficiencies. Such differences in overpass time play an important role in fire detection. MODIS AM1, with its morning and late night overpasses, will certainly miss a large number of short duration afternoon fires found in tropical South America and Africa. An improved fire detection by MODIS will be achieved after the launch of the PM platform in 2000.

The cumulative fire data described above are produced on a weekly basis for a grid with cells of 0.5 degree of latitude and longitude and is updated daily after the satellite early afternoon pass. They are available on a World Wide Web site (http://www.nma.embrapa.br/projetos/qme/queimadas.html), and is distributed to newspapers and atmospheric modelers. Other INPE operational fire products include daily maps of the AVHRR fire pixel detection over Brazil and some neighboring countries. These are found at http://condor.dsa.inpe.br/ult_focos.

Cahoon et al. (1991) examined a large fire in China using NOAA-9 data. Using 3.7 μm saturation as their detection criterion, they found good accordance with observed smoke plumes. However, Brustet et al. (1991) found in a AVHRR study in semi-arid West Africa, that a threshold in the 3.7 μm channel alone was adequate for fire detection in some cases only, while for dry vegetation with hot background soil surfaces, a second threshold applied to the 11 μm channel was necessary.

The techniques developed for vegetation fires can also be used in an urban setting, such as the fires following riots in Los Angeles in April 1992 (Doussett et al., 1993). Robinson (1991), Kennedy (1992), Justice et. al., (1993) and Cracknell (1997) all provide reviews of fire detection using AVHRR and address a number of sources of uncertainty. Although the

AVHRR was not designed for fire detection, and as pointed out suffers from several drawbacks in this regard, it provides a broad base of experience in orbital detection of vegetation fires. With over ten years of AVHRR application to fire studies, some of the results have been used to identify MODIS fire product needs and assist in their design. In particular, the global and regional fire products from the Joint Research Center, Italy and ESA-ESRIN, Italy and the operational real-time detection program of INPE, Brazil, are good indicators of the potential contribution from MODIS standard fire products.

3. MODIS Strategy for Remote Sensing of Fires

The need for better tools in assessing biomass burning from remote sensing led to the inclusion of two fire channels in the MODIS instrument (Salomonson, 1989), to be flown on the Earth Observation System (EOS) in 1998 (observations at 10:30 am and 10:30 p.m. local subsatellite time) and 2000 (observations at 1:30 p.m. and 1:30 am local subsatellite time). As opposed to the AVHRR, MODIS will be equipped with infrared (IR) spectral channels specifically designed to detect and characterize fires and their emitted thermal energy. The 4 and 11 μm channels are designed to be sensitive to temperatures reaching about 450K and 400K respectively. Therefore, except for large wild fires, these MODIS channels, with resolution of 1 km at nadir, are not expected to saturate. MODIS is planned to monitor global fire activity twice during the day (after the launch of the second platform) and twice during the night. The main remote sensing effort will be towards accurate detection of the presence of fires and their location, which will be used to monitor the frequency and spatial distribution of fires.

In addition, the detected radiation emitted from the fire at 4 μm will be used to monitor the rate of emission of thermal radiation from the fire, which is expected to be proportional to the instantaneous rate of biomass consumption by the fire, and, therefore, to the instantaneous rate of emission of trace gases and aerosol particles. The relationship between the fire IR brightness temperature at 4 μm and 11 μm, for fires with signals above the background temperature variability at 11 μm, should be an indication of the average fire temperature, and therefore, of the relative contribution of smoldering (cooler) and flaming (hotter) to the biomass consumption and their effect on the combustion efficiency and emissions as well. It should be noted that the combustion efficiency is the fraction of carbon released from the biomass in the form of CO_2 (Ward et al., 1992). Radiative processes in the fire, spatial inhomogeneity of the fire pixel and obscuration by vegetation and ash can affect measurements of the rate of emission of thermal radiative energy from the fire. Thus far, there is not enough experience to judge the accuracy of these measurements. Nevertheless, the rate of emission of thermal radiative energy will be useful to compare the strength of fires at different locations and times.

Extensive comparison between the fire thermal energy, the rate of formation of burn scars and the emission of smoke in different ecosystems, will enable "calibration" of the measured thermal energy to permit the derivation of the emissions of smoke trace gases, and particulates (Kaufman et al., 1996; 1998). The interpretation of the detected fire energy in terms of consumed biomass is complex and may vary from one vegetation type to another. The success of the MODIS algorithm and products in separating smoldering and

flaming fires or in indicating the combustion efficiency will be "calibrated" using laboratory measurements and validated in the field after launch.

The MODIS instruments alone will provide up to four observations in 24 hours. Given the limited sampling of the diurnal cycle, emission estimates may have to be based on a combination of the MODIS high resolution data and geostationary observations of fires, using a coarser spatial resolution but a higher temporal resolution (every half-hour). Currently, coverage from GOES is restricted to the North, Central and South America. However, over the next decade, METEOSAT second generation and MTSAT satellites will provide coverage of Europe, Africa, Asia, Australia and the Pacific Islands.

Two additional algorithms are under development as part of the MODIS suite of fire products for early post-launch implementation and testing. First, a simplified algorithm for MODIS near real-time volcano and fire alert is being developed by the University of Hawaii as part of a NASA EOS Interdisciplinary Science (IDS) study in conjunction with the MODIS fire team. This alert algorithm provides an initial filtering of five channels of the data stream and is designed to run at an early stage in the MODIS data chain with no other data dependencies, thus enabling rapid access to the data. The volcano and fire alert products provide the basis for a multistage sampling enabling the coarse resolution targeting of high resolution coverage from ASTER and Landsat 7. Secondly, a MODIS burn scar product is being developed to meet the needs of the emissions modeling community by providing a direct estimate of area burned. The algorithm uses a time-series analysis of the reflectance component of the MODIS 3.9 µm channel for scar identification (Roger and Vermote 1997, Roy et al. 1998, 1997, Justice et al . 1998).

4. MODIS Instrument Characteristics

The MODIS 1 km 4 µm high gain channel was specified to have a saturation level of about 450 K with NEdT of 0.3 K. This channel is not affected by water vapor absorption and is only weakly affected by other gaseous absorption (see Fig. 5).

The MODIS 11 µm channel, with a 1 km resolution, saturates at a temperature of 400 K, with NEdT of 0.1K. Detection may be also possible at night using the 0.86 µm channel which has a 250 m resolution and 2.1 µm and 1.6 µm channels, with a 500 m resolution, though there are currently no plans for routine collection of the solar channels during the night. The MODIS design tries to ensure the highest possible locational accuracy of the data to provide the best information as to the location of fires and allow multitemporal monitoring of fires. Good band to band registration (0.1 of a pixel) and scene to scene registration is required, since misregistration will lead to overestimation of fire occurrence. Because there is no possibility for on-board calibration of the fire channels at high temperatures, preflight calibration data will be used in addition to post-launch vicarious calibration using known fixed sources (e.g., gas flares).

The MODIS sensor scans the earth with ten simultaneous 1 km wide stripes (or 20 and 40 stripes at the 500 m and 250 m resolutions, respectively). The MODIS 250 m bands can be used to provide information on the spatial variability of the 1 km fire pixel and the

background surface. An inverse relationship has been established between the Normalized Difference Vegetation Index (NDVI) and surface temperature which may help with assumptions concerning background temperature. The MODIS cloud mask will be an important component of the fire detection by identifying areas where the surface is obscured by clouds and fires are undetectable. The 250 m channels will also be used to detect sub-pixel clouds within the 1 km pixel. The general design of the MODIS instrument and its application for remote sensing are described by Salomonson et al. (1989), King et al., (1992), Running et al (1994), Barnes et al., (submitted), Justice et al., (submitted). At off-nadir there is an overlap between the scan lines of different swaths. To avoid the effect of off-nadir viewing on multiplicative fire detection, the fire detection will be limited to view angles of ±45°.

The MODIS pixel size at 4 μm and 11 μm is 1 km. However, due to the scanning mode of MODIS the response is triangular across 2 km with maximum response in the center of the pixel (see Fig. 6). As a result, fires can be expected to be detected by one or two adjacent pixels depending on the location of the fire relative to the pixel and on the strength of the fire. It should be pointed out that if instead of a triangular response, the MODIS response were rectangular with no overlap, each fire would be singularly detected with a response equal to the sum of the responses of the two adjacent pixels depicted by the triangular response.

5. Spectral Properties of Fires

The MODIS algorithm is based on the spectral properties of fires in the mid and longwave IR. These properties are the result of the fire pixel inhomogeneity and the expected range of the fire temperatures. In a given fire pixel there may be areas that are not burned, are smoldering or are in flames. Figure 7 demonstrates the modeled sensitivity of the MODIS channels to the fraction of the pixel covered by flames of 1000 K (f_{flame}) and a fraction of the pixel covered by smoldering of 600K (f_{smold}). The remainder of the pixel has a temperature of 300 K. The shorter the wavelength, the stronger the sensitivity to the higher temperature region. The main results of the simulation are summarized in Table 2. The 1.65 μm channel is very sensitive to f_{flame} and the flaming energy but not very sensitive to f_{smold} and its energy. The 2.13 μm channel is very sensitive to f_{flame} and somewhat sensitive to f_{smold}. Since the thermal energy is more concentrated in the flaming fire, the sensitivity to thermal energy is independent of smoldering or flaming. Unfortunately, the MODIS 2.13 μm channel saturates at a reflectance of 0.8, which, for the low solar brightness in this channel corresponds to less than 1% of the 500 m pixel being in flames. During the day this channel is strongly affected by the reflection of sunlight. The importance of this channel is therefore limited. The 4 μm channel is the next atmospheric window. It is sensitive to both f_{flame} and f_{smold}, and is five times more sensitive to the thermal energy emitted from smoldering than flaming. The stronger sensitivity to smoldering means that, for the same apparent temperature in 4 μm measured by MODIS, the rate of emission of radiative thermal energy and the rate of combustion is higher for grassland fires than for forest fires, the latter having a much more pronounced smoldering phase (Ward et al., 1992). The reflection of sunlight in this channel is considerably less important due to the low levels of solar radiation (at 3.9 μm the sun is half as bright as at 3.75 μm used in AVHRR). It

therefore is our main channel for fire detection and characterization. Fig. 8 shows the effect of a fire size and temperature on the apparent temperature of the pixel at 4 μm. This channel is sensitive to fires as small as 10^{-4} of the fire pixel. The 4 μm channel response during daylight may be strongly enhanced by surface reflection where the satellite-surface-solar geometry results in sun glint. This effect has been documented over oceans (Nath et al., 1993; Cracknell, 1993, Setzer and Verstrate, 1994) and can lead to false fire detections over land (Setzer and Malingreau, 1996). Therefore the MODIS fire detection algorithm tests for sun glint and excludes those pixels from the fire products.

6. MODIS Fire Algorithm

The MODIS fire detection and characterization techniques are planned to be fully automated for the production of daily, global fire information. In order to detect the presence of fire in a non-interactive fashion, a set of detection criteria different for the day and night fire observations are established.

6.1 Fire Detection

The following procedure emerges from the physics of fire thermal emission discussed above and the algorithms used with currently available AVHRR and GOES data (Giglio et al., 1998). Only the procedures using the 4 μm and 11 μm bands are described. In its current form the algorithm consists of a number of threshold values. These threshold values are given for both day and night observations. During the night, the signal at 4 μm is smaller due to lack of reflection of sunlight and the thresholds are lower. The regional and seasonal variability of the land surface makes absolute thresholds insufficient. The threshold values presented below were chosen, based on the cited literature and the present remote sensing experience of the authors. The values of the thresholds determine the minimum size and energy of a fire that can be detected. The thresholds are evaluated using analyses of data from airborne instrumentation flown in the Smoke Cloud and Radiation (SCAR) experiments in the US and Brazil (Kaufman et al., 1996; 1998).

Fire detection is based on the MODIS signal at 4 μm, and is enhanced by the information at 11 μm. The fire detection strategy is based on absolute detection of the fire, if the fire is strong enough, and on detection relative to the background to account for variability of the surface temperature and reflection of sunlight. To avoid false detection, all pixels for which $T_4 < 315$ K (305 K at night) or for which the difference between the temperature at 4 μm and at 11 μm (ΔT_{41}), $\Delta T_{41} < 5$ K (3 K) are not considered as fires. For a background of 310 K at 4 μm, this corresponds to a fire size of 1000 m^2 at 600 K or 50 m^2 at 1000 K. After launch it will be checked whether these criteria result in small fires being missed in the Boreal region where surface temperatures are relatively low.

For absolute fire detection the algorithm requires that the fire apparent temperature at 4 μm is $T_4 > 320$ K (315 K at night) and $\Delta T_{41} > 20$ K (10 K at night). But if $T_4 > 360$ K (330 K at

night), the threshold for ΔT_{41} is not required. This may be important for large low temperature smoldering fires that may not have a significant spectral variability in the IR. If this criterion is not met the algorithm allows a relative fire detection in which the fire is distinguished from the background by 4 standard deviations in T_4 and by the difference ΔT_{41}:

$$T_4 > T_{4b} + 4\delta T_{4b} \text{ and } \Delta T_{41} > \Delta T_{41b} + 4\delta\Delta T_{41b}$$

where δT_{4b} is the standard deviation of the background temperature at 4 μm and $\delta\Delta T_{41b}$ is the standard deviation of the difference in the background temperature at 4 and 11 μm. δT_{4b} or $\delta\Delta T_{41b}$ need to be at least 2 K.

6.2 Rate of emission of thermal radiative energy

The total rate of emission of radiative energy from the fire, E_f, is expected to depend on the rate of combustion of biomass in the fire. The heat of combustion is divided between conductive/convective heat and radiative heat. Part of the radiative energy is emitted towards the ground and converted to conductive heat in the ground. Part of the radiative energy may be obscured by cooler material above the combustion level (e.g., ash layers or a vegetation canopy). The division between conduction, convection, and radiation can be temperature dependent. The reason why we expect the estimation of the fire radiative energy to be useful is that both the rate of emission of radiative energy and the rate of combustion are proportional to the size of the subpixel fire and to the density of the biomass burned in it. Therefore, the rate of emission of radiative energy is believed to represent the fire intensity well and to be proportional to the rate of emission of trace gases and particulates from the fire. The ratio between the radiative energy and the total combustion energy may vary between different ecosystems and fuel types and presently is not known. Using MODIS data, analysis procedures used with the AVHRR (Kaufman et al., 1990a, b) in which the emissions of particulates were estimated for a given fire region, will be followed. While for the AVHRR it is possible to relate emissions to the total number of fires, for MODIS it will be possible to relate emissions to the sum of the fire radiative energy and thus, the intensity of the individual fires will be taken into consideration.

The rate of emission of radiative energy is derived from the measured fire temperature at 4 μm, T_4. E_f, is correlated to the value of T_4 (see Fig. 9a) more than to temperature of any other channel, because this channel is sensitive to both smoldering and flaming (though more to flaming). There is only a small influence from the ratio between smoldering and flaming on the dependence of E_f on T_4 (see Figure 9a). The relationship between the emitted energy and the detected temperature in the 4 μm channel is approximated in Figure 9a by:

$$E_f = 4.34 \cdot 10^{-19}(T_4^8 - T_{4b}^8) \text{ (watt/m}^2 \text{ or MWatt per pixel)} \quad (1)$$

and is shown by the solid line. Sensitivity studies and applications of this concept are given in subsequent sections. The minimum detectable fire size of 10^{-4} of the pixel, corresponding to ΔT_4~20 K, emits energy in the rate of 10-20 MWatt. This is 100 to 1000 times smaller (more sensitive) than savanna fires measured recently in South Africa (Shea et al., 1996).

6.3 Smoldering and flaming fires

Amongst the fire characteristics planned for estimation using MODIS, the most challenging is probably the determination of the flaming and smoldering ratio. The two fire stages, flaming and smoldering, distinct for example in forest fires, are characterized by different fire intensity, temperature, combustion efficiency and emission ratios. In several field experiments in Brazil, 2-3 times more emissions of aerosol particles, CH4 and NMHC, per unit of biomass, were measured in the smoldering than in the flaming phase (Ward et al., 1992; Kaufman et al., 1992; Malingreau et al. 1993). Therefore, it is important to be able to distinguish between these two phases. Figure 10 shows the difference in the emission factors between smoldering and flaming as a function of the combustion efficiency. The data collected in the tropics represent grassland and forest fires. Their emission factors are well represented by a single line as a function of the combustion efficiency. For particulates there is also a good agreement between the measurements in the tropics and the average relationship obtained for the prescribed fires in North America (Ward and Hardy, 1991). For CH_4 there is a substantial difference in the average relationship, which is important when estimating the emissions for combustion efficiencies smaller than 0.85.

Smoldering and flaming correspond to different ranges of combustion efficiency. They can be distinguished using IR remotely sensed measurements only if the fire temperatures vary significantly between these two stages. Based on review of the fire properties presented by Lobrt and Warnatz (1993), flaming temperature can be anywhere between 800 K and 1200 K and as hot as 1800 K. Smoldering should be under 850 K and above 450 K. The actual range is probably smaller. Therefore, the algorithm and sensitivity studies should be based on the assumption that the flaming temperature is 1000 K ± 200 K and smoldering 600 K ± 100 K. Figure 9b shows a simulation of the relationship between the apparent fire temperatures at 11 µm and 4 µm and the fraction of the combustion in the smoldering phase. To distinguish between smoldering and flaming it is required that the fire apparent temperature at 11 µm is significantly larger than the background: $\Delta T_{11} = T_{11} - T_{11b} > 2\delta T_{11b}$. In addition, the minimum difference in temperature between the fire pixel and the background should be $\Delta T_{11} > 0.5$ K and $\Delta T_4 = T_4 - T_{4b} > 10$K at 11 µm and 4 µm respectively. The relationship between the apparent temperature at 11 µm and at 4 µm is used to distinguish between three possible fire phases, namely, only smoldering, only flaming and a mixture of both (see Fig. 9b). To generate a threshold that can be used to distinguish between smoldering and flaming a simulation of numerous fires with a varying fraction of smoldering and flaming was used. The average relationship between ΔT_{11} and ΔT_4 for all the data is:

$$\Delta T_{11} = 0.057 \Delta T_4^{1.1} \qquad (2)$$

and reflects the change in the fire energy. The residual: $\delta T_{11} = \Delta T_{11} / (0.0057 \Delta T_4^{1.1})$ represents the excess signal at 11 μm due to smoldering rather than flaming. It is plotted as a function of ΔT_4 in Fig. 11. The residual separates between smoldering, flaming and a mixed zone in between and is therefore, expected to be correlated with the combustion efficiency. The thresholds that separate smoldering and flaming are derived from:

If $\delta T_{11} < 1.0$K - flaming stage
If $\delta T_{11} > 1.7$K - smoldering stage
Otherwise - a mixed stage

6.4 MODIS Fire Algorithm Components

1. Cloud detection and scan angle limits: The fire information is derived for all land pixels but the presence of clouds is determined using the MODIS cloud mask. For example, thick clouds with reflectance larger than 0.2 in the 0.66 μm channel will be identified, as these clouds may not be transparent to the fire signal. The MODIS cloud product includes an assessment of the 250 m channels for the presence of clouds. A scan angle cut-off will be determined to limit problems associated with fire detection and characterization at extreme view angles (e.g., 45°).

2. Atmospheric correction: The apparent temperatures T_4 and T_{11} will be corrected for gaseous absorption including water vapor absorption at 11 μm. It should be noted that small clouds may reduce the apparent fire temperature at 11 μm and may impact the derived smoldering/flaming ratio.

3. Background characterization: The relationship between the apparent temperatures of the examined pixel and its surrounding pixels is established. The surrounding pixels are used to estimate the background temperature (or non-burning temperature) of the fire pixel. This approach assumes that the correlation between the background temperature of the fire pixel and temperatures of the surrounding pixels decreases with distance from the pixel. An expanding grid centered on the fire pixel is interrogated until a sufficient number of cloud, water or fire free pixels are identified**.**

Energetic fire pixels are eliminated from the analysis of the background characteristics and are determined as having $\Delta T_{41} = T_4 - T_{11} * 20$ K (10 K at night) and $T_4 > 320$ K (315 K at night). Excluding these energetic fires, the average background apparent temperature - T_{11b} and its standard deviation - δT_{11b} are calculated. T_{4b} and δT_{4b} are calculated in a similar way. The median temperature difference between the 11 μm and 4 μm apparent temperatures of the background, ΔT_{41b}, and the standard deviation, $\delta \Delta T_{41b,}$ are calculated.

4. Fire detection: All pixels for which $T_4 < 315$ K (305 K at night) or $\Delta T_{41} < 5$ K (3 K at night) are not considered as fires. If the standard deviations δT_{4b} and $\delta \Delta T_{41b}$ are less than 2 K, then 2 K is used instead. A pixel is defined as a fire pixel (from the remaining pixels) if one of the following five combinations of logical conditions (labeled by letters) are met:

(A) (B)

{ [($T_4 > T_{4b} + 4\delta T_{4b}$) or	$T_4 > 320$ K (315 K at night)] and	
[($\Delta T_{41} > \Delta T_{41b} + 4\delta \Delta T_{41b}$) or	$\Delta T_{41} > 20$ K (10 K)] } or	{$T_4 > 360$ K (330 K)}
(a)	(b)	(X)

5. Glint exclusion: a fire pixel is excluded during the day if it corresponds to glint measurements: $\rho_{0.64} > 0.3$ and $\rho_{0.86} > 0.3$ (a reflectance that corresponding to 312 K at 4 μm) and glint angle < 40°.

At this point processing is complete for the Level 2 MODIS fire product. Some of the Level 3 (gridded) fire products require consolidated (rather than individual) fire pixels, however, for these products several additional steps are performed. These are:

6. Consolidation: As a result of the triangular response of MODIS (Fig. 6), the same fires may be represented by two adjacent pixels in the scan direction. This will be the case especially for strong fires. Approaches are being developed to consolidate the number of fires after initial detection. One statistical approach that is currently being evaluated is outlined below and will be implemented for the MODIS 10 km gridded fire product. Since the MODIS triangular response affects the fire pixel distribution only in the scan direction and not in the track direction, significant asymmetry between the scan and track direction in the fire pixel distribution can be used as an indication that a consolidation between adjacent fire pixels is needed. The first step is to determine on a grid of 100 x 100 km: the total number of fires pixels, N_f, the number of pairs or triplets in the scan direction, N_s, and the number of pairs or triplets in the track direction, N_t. If for the pairs or triplets $N_s - N_t > 3$ and $N_s - N_t > N_f/3$ then fire consolidation is required. The detected fires are consolidated in the following way:

i) A single pixel fire detected - no consolidation

ii) Two adjacent fire pixels detected along-track. Combine the MODIS response for the fires into a single fire detection:

$$L_{4c} = L_{4\alpha} + L_{4\beta} - L_{4b} \qquad (3)$$

where, the radiance is computed from the Planck function: $L_4 = P(T_4)$, for pixel α and β. The radiance is converted to the combined temperature using the inverse Planck function: $T_{4c} = P^{-1}(L_{4c})$. The same consolidation is applied at 11 μm. L_{4b} is the background radiance at 4 μm.

iii) N adjacent pixels along track detect fires:

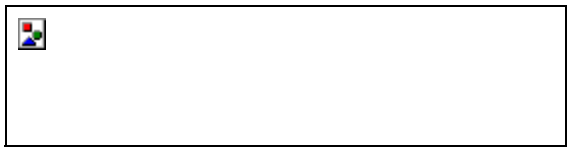

(4)

The pixel location of the fire is defined by the weighted average of the centers of the pixels, where the weights are the excess radiance at 4 μm.

7. Total rate of emission of radiative energy from the fire: The relationship between the emitted energy and the detected temperature difference in the 4 μm channel is approximated by:

$$E_f = 4.34 \cdot 10^{-19}(T_4^8 - T_{4b}^8) \text{ (watt/m}^2 \text{ or MWatt per pixel)} \quad (5)$$

8. Smoldering or flaming stage: To distinguish between smoldering and flaming it is required that:

$$\Delta T_{11} > 2\delta T_{11b},\ \Delta T_{11} > 2 \text{ K and } \Delta T_4 > 10 \text{ K}.$$

Otherwise only E_f is determined from the average relationship between T_4 and E_f. To eliminate the effect of background temperature, the apparent temperatures at 11 μm and at 4 μm are first scaled to a background temperature of 300 K and zero reflectance by subtracting the excess radiance. The thresholds that separate smoldering and flaming are derived using:

$$\delta T_{11} = \Delta T_{11} / (0.0057 \Delta T_4^{1.1}): \quad (6)$$

If $\delta T_{11} < 1.0$K - flaming stage
If $\delta T_{11} > 1.7$K - then smoldering stage
Otherwise - a mixed stage

At this point processing of consolidated fire pixels is complete. Table 3 summarizes the information collected for consolidated fire pixels. Summaries of the actual measured quantities: T_4, T_{11}, T_{4b}, T_{11b}, δT_{4b}, δT_{11b}, total emitted energy, E_f, and flaming/smoldering phase detection δT_{11} are included. Statistics on cloud obscured observations will also be stored. The information is stored separately for each of the two or four daily fire observations.

6.5 Gridded (Level 3) Fire Products

The Level 3 gridded fire products will be generated from all the individual observations stored over a 24 hour period at a Level 2 grid. A description of the MODIS gridding technique is given by Wolfe et al. (1998). The Level 2 data base will be archived and made available to the user community. The fire products will be assembled for individual days and summarized for compositing periods of eight days and one month. Gridded products will be available at full resolution (1 km) which include a record of the most-confident fire detected in each grid cell during the compositing period. Statistical summary products will

also be available at coarser 10 km and 0.5° grids. These latter products are being designed for use in regional and global modeling.

As previously described, the consolidated fire pixels will be used to generate the coarser resolution (10 km x 10 km and 0.5° x 0.5°) summary products. Each grid cell will contain a histogram classifying the fires by their 4 μm brightness temperature, T_4, which is proportional to the thermal energy. These classes are:

Class 0: $T_4 < 315$ K
Class 1: 315 K < $T_4 < 320$ K
Class 2: 320 K < $T_4 < 325$ K
Class 3: 325 K < $T_4 < 335$ K
Class 4: 335 K < $T_4 < 350$ K
Class 5: 350 K < $T_4 < 400$ K
Class 6: 400 K < $T_4 < 450$ K
Class 7: 450 K < $T_4 < 500$ K

For each class the average value of $\Delta T_{41} = T_4 - T_{11}$ will also be stored in addition to the total thermal energy emitted in the grid box and the average smoldering/total ratio, weighted by the total emitted energy.

In addition to the active fire products, current plans include providing a MODIS burned area product at a 10 km grid on an eight day and monthly basis. The product is aimed at meeting the needs of researchers developing emission inventories. The algorithm is currently under development and comparisons are being made between the use of vegetation indices, surface reflectance, surface temperature, and surface texture time-series. Emphasis is also placed on the reflectance component of the 4 μm channel at 1 km, which shows a marked contrast between fires, burn scars, and surrounding unburned areas (Roger et al. 1997, Roy et al. 1998, Justice et al. 1998).

7. Simulation Studies

Simulations are used to show the sensitivity, expected accuracy and application of the MODIS fire algorithms to synthetic data. The first example given, is a simple simulation of a mixture of smoldering, flaming and background surfaces. Several flaming and smoldering temperatures are used in the simulation, due to the uncertainty in these temperatures: smoldering - 600 K ± 100 K and flaming - 1000 K ± 200 K. The simulation, shown in Figure 12, is designed to test the possibility of distinguishing between smoldering and flaming conditions from space observations of the spectral apparent fire temperature. The simulation looks for all the possible fire characteristics at the range of temperatures described above that give the same spectral response at the 4 and 11 μm channels of the satellite sensor. For example, the open circles in Figure 12, represent fraction of the fire in the smoldering stage between 0 and 40%, and all of them give the same spectral response at 4 and 11 μm of $T_4 = 400$ K and $T_{11} = 309$ K. The simulation shows that the total emitted thermal energy can be much more accurately derived from the measurements than the ratio of the thermal energy emitted in the smoldering or flaming stages. The total emitted energy that corresponds to a given set of measurements varies by only ±10%. The ratio of the

energy emitted as smoldering to the total varies usually by ±20%, and is sufficient to distinguish only between three stages of fire: flaming, smoldering or mixed stage. Uncertainties in the assumed temperature of the smoldering and flaming stages are the main sources of uncertainty in the derived fire thermal energy and fractionation between smoldering and flaming components.

An additional source of uncertainty is the background characterization. It is possible that the background temperature of the fire that is found within the MODIS fire pixel is different from the background that MODIS senses outside of the MODIS pixel. This can happen for example, if part of the MODIS pixel was recently burned and has a warmer temperature and higher or lower reflectance at 4 μm. For the strongest fire in Fig. 12 with E_f = 1300 Mwatt, an uncertainty in the background temperature of 5 K corresponds to an error in E_f of only 2% and in the fraction of energy released in the smoldering stage of 5%. Similar errors result from uncertainty in the surface reflectance at 4 μm of $\Delta\rho_4 = 0.05$ for this fire. For fires that consume less biomass and radiate less energy it is more difficult to determine the total emitted energy and fraction of energy emitted in the smoldering phase. For the second smallest fire in Fig. 12, with E_f=230 Mwatt, the apparent temperature of the fire pixel at 11 μm is only 9 K more than the background. In this case, if the background temperature is underestimated by 5 K, the energy of the fire will be overestimated by 15% and instead of being considered as pure flaming, the fire is considered as mixed phase. For the weakest fire in Fig. 12, smoldering or flaming cannot be determined in the presence of such uncertainties in the background temperature or reflectance, but the error in total energy is only 15% for an error in background temperature of 5K. Therefore, it is concluded that uncertainties in the background reflectance and temperature can be tolerated in the derivation of the energy emitted from the fire and that it is possible to distinguish between smoldering and flaming only if the response of the temperature at 11 μm, ΔT_{11}, is at least twice as large as the uncertainty in the background temperature. The mid-IR 500 m resolution reflectance observations will be used to determine the heterogeneity of the fire pixel itself and the heterogeneity in the difference between the fire pixel and its background. This information will be included in a quality flag since the larger the heterogeneity, the larger the effect of background uncertainty on the determination of flaming and smoldering ratios.

The second simulation addresses the large spatial heterogeneity of fires. Each fire pixel was subdivided into 500 zones. The temperature of these zones is defined by three main temperatures: background, T_b, smoldering, T_s, and flaming, T_f. Each zone is randomly assigned a temperature in a Gaussian distribution around one of these three temperatures with a fixed, predetermined fraction of smoldering and flaming in the fire pixel. By varying the values of T_b within 280 - 320 K, T_s within 400 - 600 and T_f within 700 - 1300 K, and by varying the width of the distributions, a variety of conditions that simulate the natural variability can be obtained. The simulation was performed for 150 fire pixels, each one with a different average temperature and coverage of the smoldering and flaming fires. For each pixel the "true" fire energy was calculated by summing the excess energy in the 500 sub-units. The total radiometric response at 4 μm and 11 μm was also calculated and used in the empirical equation 5 to calculate the apparent fire thermal energy. Fig. 13 shows a comparison between the true and retrieved apparent fire energy. The retrieved fire energy

fits the true energy very well. The average standard deviation in deriving the fire energy is ±16%. It is larger for small fires and smaller for energetic fires (see Table 4). Inclusion of an uncertainty in surface reflectivity of sunlight between the background and the fire pixel, generated negligible errors in the derived energy for energies larger than 100 Mwatt. The error was larger for smaller fires. Table 4 summarizes the results of this simulation study.

8. MODIS Fire Product Prototyping Activities: Application To Wild And Prescribed Fires

8.1 Landsat observations of the 1988 Yellowstone Fire

The Yellowstone fire in Wyoming, Montana, and Idaho began with a series of lightning strikes on July 9 - 11, 1988 and eventually spread to engulf 5,000 km^2 in and around Yellowstone National Park (Morrison, 1993). A Landsat Thematic Mapper (TM) image was collected on September 8, 1988 at 10:30 AM and is used here to describe the wildfire and to simulate the MODIS fire observations. The Landsat TM imager has seven spectral channels, six of which have a resolution of 30 m: 0.48 µm, 0.56 µm, 0.66 µm, 0.83 µm, 1.65 µm, and 2.2 µm and one with a resolution of 120 m at 11.4 µm. Figure 14 shows the entire Yellowstone data set (216 km x 180 km) resampled to 500 m/pixel spatial resolution and converted to simulate MODIS bands 7 (red, 2.2 µm), 6 (green, 1.65 µm) and 1 (blue, 0.66 µm). The image is particularly useful for identifying a chronology of fire activity. Pink areas are regions of intense active fires, while brick-red areas represent burn scars that are one to three days old where smoldering elements and small fire pockets are still radiating significantly at 2.2 µm. Older burn scars are represented by the yellow areas in the image. Thus, MODIS channels 7, 6 and 1 could be used to estimate the extent of active fires and recent burn scars while smoke enshrouds the area of interest.

As a background to the satellite observations, the fire development of the preceding day for a small subsection of Yellowstone will be described (Figures 15 and 16, see also Flynn and Mouginis-Mark, 1995). There were two large columns of smoke and fire 5 km west and southwest of the location of the Yellowstone Old Faithful geyser twenty four hours before the Landsat TM overpass. At 3 PM on September 7 the winds began to strengthen from the southwest. At 3:30 PM the fire was close to the Old Faithful Visitor Center with enough convection to generate winds of 80 km/hr. Fire balls and flaming elements passed to the northeast of the visitor center (Morrison, 1992). This particular fork of the fire zone (shown 20 km west of Yellowstone lake in Figure 10) grew by 200 km^2 that day .

Figure 15a is a false color composite of the 11.4 µm (red), 2.2 µm (green), and 1.65 µm (blue) TM channels and shows the location of the fire and the burned area. The burn scars are warmer than the surrounding area and are therefore, shown in pink-red colors. The large burn scar in the lower right part of the image was generated by a fire storm 19 hours before the acquisition of the TM image. It is 2.1 km wide at the base and 12.7 km long. Many of the active fires located mainly along the perimeter of the burn scar saturated the 2.2 µm channel. The active fire cells appear yellow-white in the image and are relatively small (60

- 120 m) with the largest one 300 m across. Table 5 shows the typical values of reflectance at 1.6 μm and 2.1 μm and temperature at 11 μm of the yellow-white fire spots, the burn scar, and the background. Figure 15b is a composite of the 11.4 μm (red), 0.66 μm (green), and 0.48 μm (blue) channels and presents the position of the burn scars relative to the smoke plumes generated from the more intense fires. Comparison of the two figures shows the relationship between the presence of main fires and the emission of smoke.

Figure 16 shows another simulation of the MODIS response to the Yellowstone fire. Because the TM does not have a 3.96 μm channel which is the main fire channel on MODIS, its response was simulated by using the non-saturating TM channels (1.65 μm, 2.2 μm, and 11.4 μm). The figure on the left shows a false color composite of the 11.4 μm (red), 3.96 μm (green), and 1.65 μm (blue) in full TM resolution. The same color picture with the resolution reduced to 1 km this time is presented on the right. The same spatial distribution of the information is seen, though it is intuitively less clear due to the reduced resolution.

Quantitative comparison between the rate of emission of thermal energy derived from the simulated MODIS observations and the Landsat observations are shown in Figure 17. The thermal energy is derived from the simulated 3.96 μm channel in both cases using equation 4. For the TM the thermal energy was derived from individual 30 m pixels and averaged to the 1 km resolution. The thermal energy derived from the simulated MODIS image is plotted in the figure as a function of the thermal energy derived from the TM image. In Fig. 17a the MODIS data are for a hypothetical rectangular 1 km response, and in Fig. 13b for the actual MODIS instrument response (Dr. Kai Yang, personal communication, 1996) which takes into account the geometric distortion of off-nadir pixels. The plots in Fig. 17 show the effect of the reduced MODIS resolution on the detection of fires and the derivation of thermal energy. The reduced resolution retains the basic information of the thermal energy with a difference of less than 1% for fire pixels. However, there are differences between the "square" 1 km resampled pixels (Figure 13a) and the geometrically distorted pixels (Figure 17b), because in the latter case, the off-nadir fire pixels are larger than those in the first case. Thus, for a given pixel, the fire energy is spread out over a larger pixel, resulting in to lower fire energies being detected (Figure 17b).

The conclusion from this application of the MODIS concept to Yellowstone fire is that this type of wildfire will be clearly observed from MODIS and that the thermal energy can be calculated from the MODIS pixel with a high degree of accuracy. This example shows that the database of MODIS thermal energy can be very useful for comparison between fires but cannot be used in an absolute sense unless correlated with some additional quantity, such as the emission of burning products. This is the subject of the next application.

8.2 MODIS Airborne Simulator data of prescribed fires in the SCAR-C experiment

The SCAR-C (Smoke Cloud and Radiation - California) experiment was conducted in September 1994 in the Northwest US (Kaufman et al., 1996). In the experiment the entire process of biomass burning was measured including ground-based estimates of fuel consumption, airborne sampling of the smoke aerosol and trace gases, and air-borne and

spaceborne remote sensing of both the fires and the smoke. In this simulation study remote sensing data collected during the experiment by the MODIS Airborne Simulator (MAS) flown on NASA's ER-2 aircraft were utilized, to find whether there is a relationship between the fire emission of thermal energy and emission of smoke and trace gases. The MAS scans in the crosstrack direction in 35 km swaths collecting data with a nominal 45 m resolution (King et al., 1996). For SCAR-C, MAS was configured with 11 spectral channels that included the 0.66 μm, 1.6 μm and 4 μm channels used in this study. Several prescribed and wild fires were measured. The Quinault prescribed fire on the coast of Washington State (September 21, 1994) was the best measured example of the relationship between the fire rate of emission of thermal energy and the rate of emission of particulates. Both the fire thermal energy and the emission of particulates were remotely sensed by MAS. The fire thermal energy was monitored by the 1.6 μm and 4 μm channels, while emissions of smoke were measured independently, at 0.66 μm, downwind from the fire. The fuel of the Quinault fire consisted of dry remnants of large western red Cedar debris, left over from logging. The density of the fuel including the deep forest floor of accumulated woody material, was 38 kg/m^2, about half of it (22 kg/m^2) was consumed in the burn according to a US Forest Service report. The burn site was reported by the US Forest Service to be 0.2 km^2, while remote sensing at 4 μm found a similar size of 0.25 km^2. The fire was ignited by heliotorch at 18:10 GMT, burned immediately vigorously and continued for about 6 hours.

The ER-2 flew over the fire eight times and generating each time an image of the size and apparent temperature of the fire as well as an image of the smoke plume. Figure 18 shows the first such remote sensing image taken from the ER-2 of the fire temperature and the emitted smoke. The size of the fire was monitored using the 4 μm channel which proved to be the most sensitive to the temperature anomaly. However, this MAS channel saturated at 450 K. As a result, the fire thermal energy was monitored by a combination of the 4 μm channel and the 1.6 μm channel at the MAS resolution. Since the 1.6 μm channel is sensitive only to temperatures above 620K, there is a gap between the two channels with low sensitivity. The MAS 1.6 μm channel saturated at 860K. For the high spatial resolution of the imagers, this channel is very sensitive to the presence of flaming and gives a high resolution image of the fire. The use of the 1.6 μm channel is different from that of the MODIS 4 μm channel, but demonstrates the derivation of the rate of emission of thermal energy. This channel was calibrated on the ground before flight and the calibration was compared and updated using simultaneous AVIRIS data.

Application of the MAS images of the fire and smoke acquired in the Quinault fire are shown in Figure 19. The figure shows the rate of emission of thermal energy from the fire and the rate of emission of particulates. The rate of emission of thermal energy is calculated from the difference between the detected radiance at 1.6 μm and the radiance due to reflection of sunlight. It is converted to the rate of emission of thermal energy assuming that each 45 m pixel is a homogeneous black body. The procedure by Fraser et al. (1984) that was developed to calculate of the flux of sulfate exiting the U.S. coast to the Atlantic was followed to calculate the rate of smoke emission. The average smoke brightness at 0.66 μm was converted into the smoke optical thickness using a radiative transfer lookup table that describes the relationship between the optical thickness and the upward radiance at the top of the atmosphere for a plane parallel smoke model (Kaufman et al., 1996). The smoke optical thickness (τ) was converted to the smoke mass density (M) using a conversion

factor of ζ=0.11 g/m^2 for the dry part of the smoke ($M=\zeta\tau$, Kaufman et al., 1990a). The rate of emission was calculated for an average wind speed of 7±2 m/s. The wind speed was obtained from six consecutive observations from the MAS images of the distance of the edge of the smoke plume from the fire. Figure 19 shows that the rate of emission of smoke and the rate of emission of thermal energy evolve as a function of time in a remarkably similar way. This implies that at least in the case of this fire, there was a direct relationship between the rate of emission of thermal radiation from the fire and the rate of emission of smoke. The same procedure will be applied to the rest of the fires measured during the SCAR-C experiment and to hundreds of fires in Brazil measured during the SCAR-B experiment in 1995. In addition, laboratory fires in a controlled environment will be used to establish the relationship between the fire thermal energy and rate of emission of aerosol and trace gases.

8.3 AVHRR prototyping of MODIS global active fire products.

The International Geosphere Biosphere Program (IGBP) Global 1km Project provides an important data base for prototyping MODIS products and is described by Townshend et al (1994) and Eidenshink and Faundeen (1994). The data are being collected from a number of ground stations around the world contributing to a global archive. As part of the NASA EOS program the global daily AVHRR data have been compiled at the Eros Data Center from April 1992 to the present.

As discussed in Section 2, the daily AVHRR orbits can be processed to identify actively burning fires and map their global distribution. An example of such application was generated by the Global Inventory Monitoring and Modeling Studies group at NASA/GSFC. Figure 20 shows the global AVHRR distribution of fires for June 21, 1992. Since 1992, the IGBP-DIS Fire Working Group (FWG) has been working to develop a community consensus on AVHRR processing for fire detection. Following recommendations from the FWG, researchers in the FIRE Project at the Joint Research Centre (JRC) in Ispra have developed a system for generating global fire products based on AVHRR from the IGBP Global 1 km Project. A global fire product developed has generated using eighteen months of daily AVHRR data (Dwyer et al., 1997). The resulting data set is currently being evaluated by the FWG and will provide a useful tool to evaluate the global distribution and timing of fires to be identified by the MODIS.

9. Concluding Remarks

The MODIS fire products are expected to provide advances in the monitoring of global fires and detection of changes in the location, density and rate of biomass consumption by fires over the globe. For large fires, for which the response in 11 μm is significantly above the background, MODIS should be able to distinguish between smoldering stage and new flaming stages. This may be important for observations of the behavior of wild fires. MODIS will generate daily, eight day and monthly composites of fire statistics. In addition

to the fire occurrence and location, the thermal signature will be used to detect the apparent radiative thermal energy emitted from the fire and to provide a rough estimate of the ratio between the energy partition between smoldering and flaming. It is known that the remotely sensed thermal energy is proportional to the rate of consumption of biomass in the fire, a parameter that is useful for estimating the magnitude of biomass burning. But there is still a need to quantify the relationship between them. The spatial distribution of the fire temperature in the MODIS pixel and obstruction of the radiative flux will affect this relationship as will the distribution of material in the fire bed with its effect on the competition between radiation and conduction/convection in redistributing the thermal energy. It is expected that these properties will be repeated in similar fuel types and that therefore, it will be possible to establish the empirical relationship between the remotely sensed thermal energy and the emission of particulates and trace gases from the fire. Establishing this relationship would be a major advance over the estimation of the average amount of particulates emitted per fire derived from the AVHRR (Kaufman et al., 1990a). These relationships will be established in laboratory measurements that simulate fires from different ecosystems before the launch of MODIS.

The recent SCAR field experiments, in the Northwest US and in Brazil, using an aircraft version of the MODIS instrument, have started to establish these basic relationships and to test the MODIS fire algorithms (Kaufman et al., 1996, 1998). In the remaining time before the launch, it is planned to continue with data simulations, controlled laboratory experiments and aircraft data analysis. In the post-launch period, emphasis will be placed on product evaluation and on conducting field validation experiments in a variety of ecosystems. One such campaign is planned for Southern Africa starting in 1999. and will build on the EOS validation program in Southern Africa and the scientific findings of the 1992 Southern African Fires and Atmosphere Research Initiative (SAFARI).

Acknowledgments

The authors wish to thank B.-C. Gao for his recommendation for the spectral location of the MODIS fire channel. R. Kleidman, B.-C. Gao, R.-R. Li, A. Chu and contributed calculations and valuable comments to the manuscript. Material from the IGBP-DIS Fire Algorithm Workshop Report contributed to the background information in this paper.

References

Andreae M.O., Fishman J., Garstang M., Goldammer J.G., Justice C.O., Levine J.S., Scholes R.J., Stocks B.J. and Thompson A. M., 1994. Biomass burning in the global environment: first results from the IGAC/BIBEX Field Campaign STARE/TRACE-A/SAFARI-92. In: *Global Atmospheric-Biospheric Chemistry*. Ed. Prinn R, Plenum Press, New York, 83-101.

W.L. Barnes, T. S. Pagano, and V. V. Salomonson. Pre-launch performance of the moderate resolution imaging spectroradiometer (MODIS) on EOS AM-1. *IEEE Trans. Geoscience and Remote Sensing* (submitted)

Brustet, J.M., J.B. Vickos, J. Fontan, K. Manissadjan, A. Podaire, and F. Lavenu, 1991, Remote Sensing of Biomass Burning in West Africa with NOAA-AVHRR, In: *Global Biomass Burning*, J. S. Levine (ed.), The MIT Press, Cambridge, Massachusetts, pp.47-52.

Cahoon, D.R., Jr., J.S. Levine, W.R. Cofer III, J.E. Miller, P. Minnis, G.M. Tennille, T.W. Yip, B.J. Stocks, and P.W. Heck, 1991. The Great Chinese Fire of 1987: A View from Space, In: *Global Biomass Burning*, J. S. Levine (ed.), The MIT Press, Cambridge, Massachusetts, pp.61-66.

Cahoon, D.R., Jr., B.J. Stocks, J.S. Levine, W.R. Cofer III, J.E., O'Neill, K.P. 1992. Seasonal distribution of African savanna fires. *Nature,* v. 245, p. 812-815.

Cracknell, A.P., 1993, A method for the Correction of Sea Surface Temperatures derived from satellite thermal infrared data in an area of Sunglint, *Int. J. Remote Sensing*, 14:3-8.

Cracknell, A.P., 1997, *The Advanced Very High Resolution Radiometer*. Taylor and Francis, U.K. pp. 533.

Crutzen, P.J., L.E. Heidt, J.P. Krasnec, W.H. Pollock, and W. Seiler, 1979, Biomass burning as a source of atmospheric gases: CO, H2, N2O, NO, CH3Cl, and COS, *Nature*, 282:253-256.

Crutzen, P. J. and M. O. Andreae, 1990, Biomass burning in the tropics: impact on atmospheric chemistry and biogeochemical cycles, *Science*, 250:1669-1678.

Dickinson, R.E., 1993, Effect of fires on global radiation budget through aerosol and cloud properties, In: *Fire in the Environment: The Ecological, Atmospheric, and Climatic Importance of Vegetation Fires*, P.J. Crutzen and J.G. Goldammer (eds.), John Wiley & Sons, New York, pp. 107-122.

Dousset, B., P. Flament and R. Bernstein, 1993, Los Angeles Fires Seen from Space, *EOS Transactions*, American Geophysical Union, 74(3):33-38.

Dozier, J., 1981, A method for satellite identification of surface temperature fields of subpixel resolution, *Remote Sensing of Environment*, 11:221-229.

Dwyer E., Gregiore J.-M., and Malingreau J.P., 1997. 'Global distribution and characterization of vegetation fires using NOAA AVHRR data'. In: Earth Surface Remote Sensing. Cecchi G., Engman E.T., Zilioli E. (editors). Proceedings of SPIE Vol.3222, pp. 76-88.

Eidenshink J. and J.L. Faundeen 1994. The 1km AVHRR global land data set: first stages in implementation. International Journal of Remote Sensing, 15, 17, 3443-3462.

Elvidge, C.D., Kroehl H.W., Kihn E.A., Baugh K.E., Davis E.R., Hao W.M., 1996. Algorithm for the retrieval of fire pixels from DMSP Operational Linescan System. In: *Global Biomass Burning*, J.S. Levine (Ed), The MIT Press, Cambridge, Massachusetts p.73-85.

Flannigan, M.D., 1985, Forest Fire Monitoring Using the NOAA Satellite Series, M.S. Thesis, Department of Atmospheric Sciences, Colorado State University, Fort Collins, Colorado, 59.

Flannigan, M.D. and T.H. Vonder Haar, 1986, Forest fire monitoring using NOAA satellite AVHRR, *Canadian Journal of Forest Research*, 16:975-982.

Flynn, L. P., and P. J. Mouginis-Mark, 1995, A comparison of the thermal characteristics of active lava flows and forest fires, *Geophys Res Lett*, 22:2577-2580.

Fraser, R.S., Y.J. Kaufman and R.L. Mahoney, 1984, Satellite measurements of aerosol mass and transport, *J. Atmos. Environ*., 18:2577-2584.

Giglio L., Kendall J. D., Justice C. O., 1998. Evaluation of global fire detection algorithms using simulated AVHRR infrared data. *International Journal of Remote Sensing* (in press)

Hansen J.E. and A.A. Lacis, 1990, Sun and dust versus greenhouse gases: an assessment of their relative roles in global climate change, *Nature*, 346: 713-719.

Hao, W.M. and M.-H. Liu, 1994, Spatial and temporal distribution of tropical biomass burning, *Global Biog. Cycles*, 8:495-503.

Hobbs, P.V. and L.F. Radke, 1969, Cloud condensation nuclei from a simulated forest fire, *Science*, 163:279-280.

Hobbs, P. V., J. S. Reid, R. A. Kotchenruther, R. J. Ferek, and R. Weiss, Direct radiative forcing by smoke from biomass burning, *Science, 275,* 1776-1778, 1997.

IPCC Climate Change 1995, Eds: J.T. Houghton, L.G. Meira Filhno, J.B. Hoesung Lee, B.A. Callander, E. Haites, N. Harris, and K. Maskell, Cambridge University Press, Cambridge.

Justice C.O., J.D. Kendall, P.R. Dowty and R.J. Scholes, 1996. Satellite remote sensing of fires during the SAFARI campaign using NOAA advanced very high radiometer data, *J. Geophys. Research* 101:23851-23863

Justice, C. O., J.-P., Malingreau, and A. W. Setzer, 1993. Satellite remote sensing of fires; potential and limitations, in *Fire in the Environment*, edited by P. J. Crutzen and J.G. Goldammer, pp.77-88, John Wiley and Sons Ltd.

Justice C.O. (ed.) 1998. The Moderate Resolution Imaging Spectroradiometer (MODIS): land remote sensing for global change research. *IEEE Trans. Geoscience and Remote Sensing* (in press).

Kaufman, Y.J. and T. Nakajima, 1993, Effect of Amazon smoke on cloud microphysics and albedo-analysis from satellite imagery. *J. Applied Meteorology*, 32:729-744.

Kaufman, Y.J., A. Setzer, C., C.J. Tucker, M.C. Pereira and I. Fung, 1990a, Remote Sensing of Biomass Burning in the Tropics, In: *Fire in the Tropical Biota: Ecosystem Processes and Global challenges*, J.G. Goldammer (ed.), Springer-Verlag, Berlin, 371-400.

Kaufman, Y. J., C. J. Tucker and I. Fung, 1990b, Remote Sensing of Biomass Burning in the Tropics, *Journal of Geophysical Research*, 95(D7):9927-9939.

Kaufman, Y. J. and R. S. Fraser, 1997, The effect of smoke particles on clouds and climate forcing. *Science*, 277, 1636 - 1639.

Kaufman, Y. J., A. Setzer, D. Ward, D. Tanre, B. N. Holben, P. Menzel, M. C. Pereira and R. Rasmussen, 1992, Biomass Burning Airborne and Spaceborne Experiment in the Amazonas (BASE-A). *Journal of Geophysical Research.*, 97:14581-14599.

Kaufman, Y. J. , B. N. Holben, D. Tanré and D. Ward, 1994, Remote Sensing of Biomass Burning in the Amazon, *Special Issue on Remote Sensing of the Amazon in Rem. Sens. Rev.*, 10:51-90.

Kaufman, Y. J. , R. Kleidman, M. D. King, and D. E. Ward, SCAR-B Fires in the tropics: Properties and their remote sensing from EOS-MODIS, *J. Geophys. Res.*, this issue, 1998.

Kaufman, Y. J., L. A. Remer, R. D. Ottmar, D. E. Ward, R. .-R. Li, R. Kleidman, R. S. Fraser, L. Flynn, D. McDougal, G. Shelton, Relationship between remotely sensed fire intensity and rate of emission of smoke: SCAR-C experiment, *Global biomass burning,* J. Levin, Ed. p. 685-696, The MIT press, Cambridge MA, 1996.

Kendall J.D,. Justice C.O., Dowty P.R., Elvidge C.D. and Goldammer J.G. 1997. Remote Sensing of Fires in Southern Africa during the SAFARI 1992 Campaign. In: van Wilgen, B.W., M.O. Andreae, J.G. Goldammer, and J.A. Lindesay (Eds.) *Fire in Southern African Savannas: Ecological and atmospheric perspectives*, Witwatersrand University Press, Johannesburg, pp. 89-133.

Kennedy, P.J., 1992, Biomass burning studies: the use of remote sensing, *Ecological Bulletins*, 42:133-148.

King, M. D., Y.J. Kaufman, P. Menzel and D. Tanré, 1992, Remote Sensing of Cloud, Aerosol, and Water Vapor Properties from the Moderate Resolution Imaging Spectrometer (MODIS), *IEEE J. Geosc. and Rem. Sens.*, 30:2-27.

King, M. D., W. P. Menzel, P. S. Grant, J. S. Myers, G. T. Arnold, S. E. Platnick, L. E. Gumley, S. C. Tsay, C. C. Moeller, M. Fitzgerald, K. S. Brown and F. G. Osterwisch, 1996: Airborne scanning spectrometer for remote sensing of cloud, aerosol, water vapor and surface properties. *J. Atmos. Oceanic Technol*., 13, 777-794.

Langaas, S. and K. Muirhead, 1989. Monitoring bushfires in West Africa by weather satellites. Proceedings of the 22nd International Symposium on Remote Sensing of Environment, October 20-26, Abidjan, Cote d'Ivoire, (253-268).

Lee, T. F. and P. M. Tag, 1990, Improved Detection of Hotspots using the AVHRR 3.7-µm Channel, *Bulletin of the American Meteorological Society*, 71(12):1722-1730.

Lobert, J.M., and J. Warnatz, 1993, Emissions from the combustion process in vegetation, In: *Fire in the Environment: The Ecological, Atmospheric, and Climatic Importance of Vegetation Fires*, P.J. Crutzen and J.G. Goldammer (eds.), John Wiley & Sons, New York, pp. 15-38.

Malingreau, J.P., F.A Albini, M.O. Andrae, S. Brown, J.L. Levine, J.M. Lobert , T.A. Kuhlbusch, L. Radke, A. Setzer, P.M. Vitousek, D.E. Ward and J. Warnatz. 1993. In: Fire in the Environment. P.J. Crutzen and J.G. Goldammer Eds., Wiley and Sons, Chichester, England, 329-343.

Matson, M. and J. Dozier, 1981, Identification of subresolution high temperature sources using a thermal IR sensor, *Photo. Engr. and Remote Sensing*, 47(9):1311-1318.

Matson, M. and B. Holben, 1987, Satellite detection of tropical burning in Brazil, *Int. J. Remote Sensing*, 8(3):509-516.

Matson, M., S.R. Schneider, B. Aldridge and B. Satchwell, 1984, Fire Detection Using the NOAA-Series Satellites, NOAA Technical Report NESDIS 7, 34.

Matson, M., G. Stephens and J. Robinson, 1987, Fire detection using data from the NOAA-N satellites, *Int. J. Remote Sensing,* 8(7):961-970.

McClain, E.P., W.G. Pichel and C.C. Walton, 1985, Comparative Performance of AVHRR-Based Multichannel Sea Surface Temperatures, *Journal of Geophysical Research*, 90(C6):11587-11601.

Menzel, W.P., and E.M. Prins, 1996: Monitoring biomass burning with the new generation of geostationary satellites. Accepted for publication in Biomass Burning and Global Change, J.S. Levine (Ed.), Cambridge MA, The MIT Press. pp. 56-64.

Morrison, M., 1993, *Fire in Paradise*, Harper Collins, New York, 253 p.

Muirhead, K. and A.P. Cracknell, 1984, Identification of gas flares in the North Sea using satellite data, *International Journal of Remote Sensing,,* 5(1):199-212.

Nath, A. Narendra, M.V. Rao and K.H. Rao, 1993, Observed high temperatures in the sunglint area over the ocean. *International Journal of Remote Sensing,* 14(5):849-853.

Penner, J. E., R. E. Dickenson, and C. A. O'Neill, 1992: Effects of aerosol from biomass burning on the global radiation budget. *Science*, 256:1432-1434.

Pereira, M.C. and A.W. Setzer, 1993, Spectral characteristics of deforestation fires in NOAA/AVHRR images, *Int. J. Remote Sensing*, 14(3):583-597.

Pereira, A.C. Jr., A.W. Setzer and J.R. dos Santos, 1991, Fire Estimates in Savannas of Central Brazil with Thermal AVHRR/NOAA Calibrated by TM/Landsat, Proceedings of the 24th International Symposium on Remote Sensing of Environment, Rio de Janeiro, Brazil, 27-31 May 1991.

Prins, E. M. and W.P. Menzel, 1992, Geostationary satellite detection of biomass burning in South America, *Int. J. Remote Sensing,* 13:2783-2799.

Prins, E.M. and W.P. Menzel, 1994, Trends in South American biomass burning detected with the GOES visible infrared spin scan radiometer atmospheric sounder from 1983 to 1991, *J. Geoph. Res,* 99:16719-16735.

Prins, E.M., and W.P. Menzel, 1996a: Investigation of biomass burning and aerosol loading and transport utilizing geostationary satellite data. In: Biomass Burning and Global Change, J.S. Levine (Ed.), Cambridge MA, The MIT Press. pp. 65-72.

Prins, E.M., and W.P. Menzel, 1996b: Monitoring biomass burning and aerosol loading and transport from a geostationary satellite perspective. Seventh Symposium on Global Change Studies, Atlanta, GA, Jan.28 - Feb.2, 1996, pp. 160-166.

Robinson, J M., 1991, Problems in global fire evaluation: Is remote sensing the solution?, In: *Global Biomass Burning*, MIT Press, J. S. Levine (ed.), Cambridge, USA, 67-73.

Radke, L.F., D.A. Hegg, P.V. Hobbs, J.D. Dance, J.H. Lyons, K.K. Laursen, R.E. Weiss P.J. Riggan and D.E. Ward, 1991, Particulate and trace gas emissions from large biomass fires in North America. In: *Global Biomass Burning*, MIT Press, J. S. Levine (ed.), Cambridge, USA, 209-224.

Roger J. C and E. F. Vermote 1997. Computation and use of the reflectivity at 3.75 microns from the AVHRR channels. Remote Sensing Reviews, 15, 75-98.

Roy, D.P., J.K. Kendall, J.M.C. Pereira, C.O. Justice, 1997, A multitemporal analysis of the use of the mid-IR in spectral vegetation indices for operational burned area mapping, *Proceedings of RSS97: Observations and Interactions,* 23rd Annual Conference and Exhibition of the U.K. Remote Sensing Society, The University of Reading, 2-4 September 1997, p.177-180

Roy, D.P., Giglio, L, Kendall, J.K., Justice, C.O., 1998. Multitemporal Active-Fire Based Burn Scar Detection Algorithm. International Journal of Remote Sensing Letters (submitted).

Running, S.. W., C.O. Justice, V. Salomonson, D. Hall, J. Barker, Y.J. Kaufman, A.H. Strahler, A.R. Huete, J.P. Muller, V. Vanderbilt, Z.M. Wan, P. Teillet and D. Carneggie, 1994,Terrestrial remote sensing science and algorithms planned for EOS/MODIS, *Int. J. Rem. Sens.*, 15: 3587-3620.

Salomonson V.V., W.L. Barnes, P.W. Maymon, H.E. Montgomery and H. Ostrow, 1989, MODIS: Advanced Facility Instrument for Studies of the Earth as a System, *IEEE Trans. on Geosc. and Rem. Sens.*, 27:145-153.

Skole D., B. Moore, W. Chomentowski, 1994. Spatial analysis of land cover change and carbon flux associated with biomass burning in Brazil 1970-1980. In R. Zepp (Ed), *Climate biosphere interaction*. John Wiley and Sons, NY. 161-202.

Scholes R.J., D.E. Ward and C.O. Justice, 1996, Emissions of trace gases and aerosol particles due to biomass burning in southern hemisphere Africa - *J. Geophys. Research*, 101:23677-23682.

Setzer, A.W. Operational satellite monitoring of fires in Brazil. International Forest Fire News, FAO-UN, (9):8-11, 1993.

Setzer, A.W.; Malingreau, J.P. AVHRR monitoring of vegetation fires in the tropics: towards a global product. In: *Biomass Burning and Global Change*, ed. J.S. Levine, chap.3, MIT Press, 48-81, in press, 1996.

Setzer, A. W. and M. C. Pereira, 1991, Amazonia Biomass Burning in 1987 and an Estimate of Their Tropospheric Emissions, *Ambio*, 20(1):19-22.

Setzer, A.W., and M.M. Verstraete, 1994: Fire and glint in AVHRR's channel 3: A possible reason for the non-saturation mystery. *Int. J. Rem. Sens.,* 15:711-715

Shea R.W., B.W. Shea, J.B.Kauffman, D.E. Ward, C.J. Haskins and M.C. Scholes, 1996. Fuel biomass and combustion factors associated with fires in savanna ecosystems of South Africa and Zambia, *J. Geophys. Research* 101:23551-23568.

Stephens, G. and M. Matson, 1989, Fire Detection Using the NOAA-N Satellites, Presented at the 10th Conference on Fire and Forest Meteorology, April 17-21, Ottawa, Canada.

Thompson A. M.. 1996. Biomass burning and the atmosphere: accomplishments and research opportunities. *Atmospheric Environment* 30, 19, i-ii

Thompson A. M., T. Zenker, G.E. Bodeker and D.P. McNamara, 1997. Ozone over Southern Africa: patterns and influences. In: van Wilgen, B.W., M.O. Andreae, J.G. Goldammer, and J.A. Lindesay (Eds.) *Fire in Southern African Savannas: Ecological and atmospheric perspectives*, Witwatersrand University Press, Johannesburg, pp.185-212.

Townshend J.R.G., Justice C.O., Skole D. , Malingreau J.P. , Cihlar J., Teilliet P., Sadowski F. and Ruttenberg S. 1994. The 1 km resolution global data set: needs of the International Geosphere Biosphere Program. *International Journal of Remote Sensing.*15, (17), 3417-3442.

Ward, D.E. and C.C. Hardy, 1991. Smoke emissions from wildland fires. *Environment International,* 17, 117-134.

Ward, D.E., R. Susott, J. Kauffman, R. Babbitt, B. N. Holben, Y.J. Kaufman, A. Setzer, R. Rasmussen, D. Cumming and B. Dias, 1992: Emissions and burning characteristics of biomass fires for cerrado and tropical forest regions of Brazil - BASE-B experiment, *J. Geophys. Res*., 97: 14601-14619.

Ward, D.E., W.M. Hao, R.A. Susott, R. Babbitt, R.W. Shea, J. B. Kauffman and C.O. Justice, 1996: Effect of fuel composition on combustion efficiency and emission factors for African savanna ecosystems, *J. Geophys. Res.*, 101, 23569-23576.

Warner, J., and S. Twomey, 1967: The production of cloud nuclei by cane fires and the effect on cloud droplet concentration. *J. Atmos. Sci.*, 24: 704-706.

Wolfe R. E., Roy D.P. Vermote E. 1998. The MODIS Land data storage, gridding and compositing algorithm: level 2 grid. *IEEE Trans. Geoscience and Remote Sensing* (submitted)